

84

Modelling the meteorology of Perth photochemical smog events

Dr Peter Rye



Department of Environmental Protection
Perth, Western Australia
Technical Series 84
April 1996

ISBN 0 7309 8080 4

Contents

1. Introduction	1
2. Descriptive Meteorology of Perth Smog Events	1
3. Description of the Meteorological Model.....	2
4. Case Studies.....	5
4.1. 4 February 1994	5
4.2. 18 March 1994	7
5. Discussion.....	9
6. Conclusions	10
7. References.....	10
APPENDIX	11

1. Introduction

In 1989 the W.A. Department of Environmental Protection established an air quality monitoring station Caversham (See figure 1). The purpose of this station was to measure concentrations of ozone and nitrogen oxides downwind of the city, in conditions with potential to generate photochemical smog.

Measured hourly averages of ozone in excess of 80 ppb (Canadian / W.H.O. acceptable limit) indicated that Perth was experiencing at least the beginnings of photochemical smog. The Perth Photochemical Smog Study was subsequently undertaken by Western Power and the Department of Environmental Protection, to provide a detailed understanding of the occurrence of smog events, over the whole of the Perth region.

The major components of the study included the continuous monitoring of photochemical smog species (at the Caversham site, and shaded sites in figure 1) and of meteorological variables, the development of an emissions inventory, and adaptation of existing computer models to represent the transport and photochemistry of smog in the region. In addition, a major field measurement exercise was conducted through the summer of 1993-1994, with the aim of characterising in detail a number of photochemical smog events.

This paper describes meteorological modelling studies using data from the 1993-1994 summer. Particular attention is devoted to the role of the Western Australian coastal low pressure trough in controlling the transport of photochemical smog and its precursors.

Meteorological fields simulated using the model described below were used in some air quality modelling during the study (Rye, 1996). In that work, the results obtained using modelled and interpolated measurements were compared. It was found that, on many days of interest, a combination of well-located measurements and a relatively simple meteorological regime meant that sufficiently accurate input data could be obtained from measurements. Because of the amount of work required to obtain a good match between modelled and measured meteorology, interpolated meteorological fields were normally used to provide air quality model input.

2. Descriptive Meteorology of Perth Smog Events

Experience through the Perth Photochemical Smog Study has shown that elevated smog concentrations generally occur when a coastal low pressure trough is present offshore (e.g., figure 2). This trough is a normal feature of the West Australian summer weather pattern (e.g., Keppert and Smith, 1992). Under these conditions, winds at the coast are generally easterly to

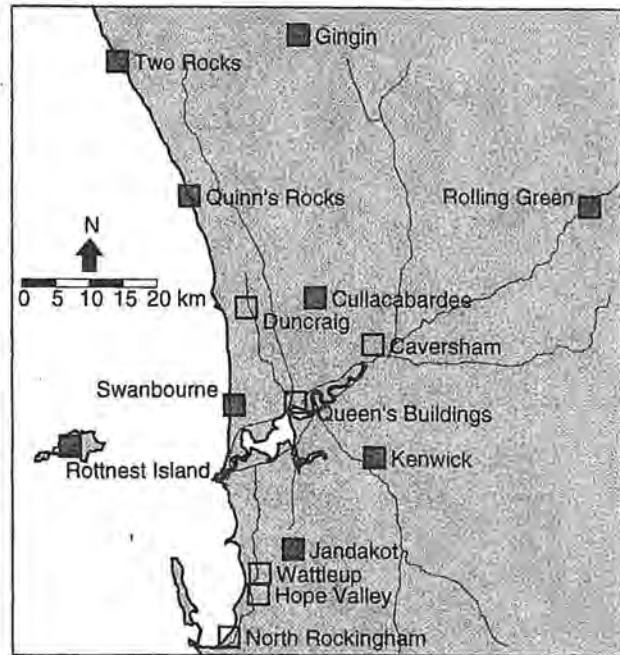


Figure 1. Air quality monitoring sites operated by the W.A. Department of Environmental Protection. Sites shown shaded were installed specifically for the Perth Photochemical Smog Study.

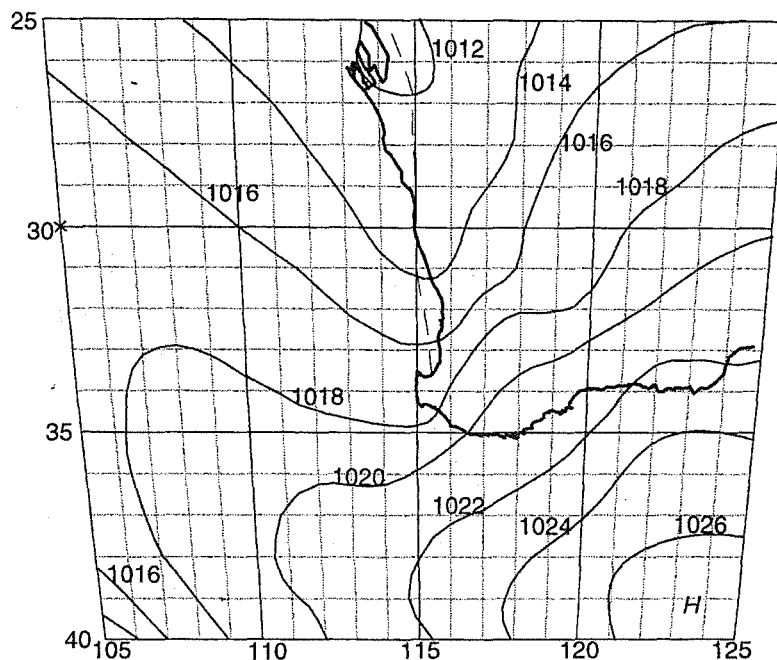


Figure 2. Surface pressure analysis for 6 a.m. WST on 16 March 1994

north easterly, so that morning emissions of smog precursors are carried offshore. When a sea breeze forms, typically in the late morning, the air mass containing the forming smog is returned to the coast. Since the sea breeze direction is normally south westerly, the air passes back over the city, accumulating further urban emissions, and peak ozone concentrations develop downwind of the central business district, typically at about 3 p.m.

The trough has a further important role in the process, due to the persisting temperature gradients between the continental air mass to the east of its axis and more maritime air in the southerly flow to the west. When a sea breeze forms, the onshore flow develops first at this temperature front, which may be 20 km or more offshore. The light winds in the transition region, from north easterly to southerly directions, ensure that urban emissions do not escape, and the advance of the sea breeze eastward into this region means that they are efficiently returned to the coast.

By contrast, when a trough is not present, morning emissions may travel offshore without impediment. Commonly, in these conditions, the sea breeze forms at the coast, and grows landward and seaward from there. This means that onshore flow in the region to which emissions have travelled may form too late to return them to the coast.

For these reasons, the meteorological modelling conducted as a component of the study has focussed mainly on the representation of the coastal trough, and its effects on windfields in the Perth region.

3. Description of the Meteorological Model

The model is an extension of that described by Rye (1989). Apart from conversion to three dimensions, several improvements have been incorporated to permit successful modelling of larger-scale wind fields. A detailed review of the model is provided in the Appendix.

The model was initially run using information from a single vertical wind and temperature profile. The sounding used a combination of the measurements available from the DEP's own

monitoring, and the Bureau of Meteorology's radiosonde releases from Perth Airport. Sodar winds, and radar winds and temperatures, were measured routinely at the Cullacabardee site, and radiosonde releases from Rottnest Island, Swanbourne and Rolling Green provided additional data on selected occasions (See figure 1 for site locations). Airport measurements were primarily used to add details at levels above 2 km, lower-level values being suspect due to the effects of the nearby Darling Scarp (Pitts and Lyons, 1988).

Initially, these data were used to create a single vertical profile of each of wind and temperature, from which uniform initialisation fields were developed. It was found that, from this initial state, the model could run stably for at least seven days. But, even when a computational grid about 1500 km square was used, a realistic coastal trough was not produced. It was concluded that production of the trough involved synoptic-scale pressure patterns. The model's initialisation was therefore altered to permit their inclusion.

The initial surface pressure gradients were specified as gradient winds in rectangular regions, covering the model grid. Cross-boundary velocity components were matched to prevent spurious convergences. In creating the initial field of wind velocities, those over the nominal site of the radiosonde release (Perth Airport) were unaltered. However, at all other grid points, the difference between the local gradient wind velocity and that at the radiosonde location was added to all initial velocities. This approach maintained the same vertical wind shear at all points, so no changes in horizontal temperature gradients were needed to maintain geostrophic balance.

A typical use of this scheme involved a trough axis aligned north-south, about 30 to 60 km offshore. Wind velocities east of the trough were set to those of the measured profile. The surface gradient wind in this region was chosen using the Bureau of Meteorology's manual surface pressure analysis, at the analysis time nearest the model start time. For the region west of the trough, a gradient wind was chosen which possessed an equal easterly component, and a southerly component representative of winds to the west of the trough.

In one variation of this scheme, gradient winds in the western region were turned easterly or north easterly, simulating the limited westward extent of the trough. In other runs, westerly gradient winds were imposed in the southern region of the model grid, representing the westerlies to the south of the sub-tropical high pressure ridge. In all cases, the aim in choosing the initial pressure field was to replicate as closely as possible the measured pressures at 6 a.m. on the second day of the model run.

Using this initialisation, small irregularities developed at the start of the model run, but dissipated as the modelled fields stabilised into a realistic form.

Figure 3 shows an example of surface pressures calculated by the model. The region in figure 3 was formed from a grid of size 120 points west-east, and 30 points south-north, with respective resolutions 12 and 40 km. The initialisation used a nominal trough axis aligned north-south, 12 km inland at Perth. The initial surface gradient wind east of the trough axis in the southern portion of the grid was 20 kt from direction 60° , and west of the axis was 20 kt from 120° . In the northern portion, winds were 14.14 kt from 60° and 120° respectively (figure 3a).

By hour 30 of the run, at 6 a.m. local time on the second day (figure 3(b)), a common form of the trough had developed, aligned from inshore in the north to offshore in the south. In the afternoon, at hour 42 (6 p.m., figure 3(c)) the trough had moved inland, under the influence of the sea breeze pressure cycle.

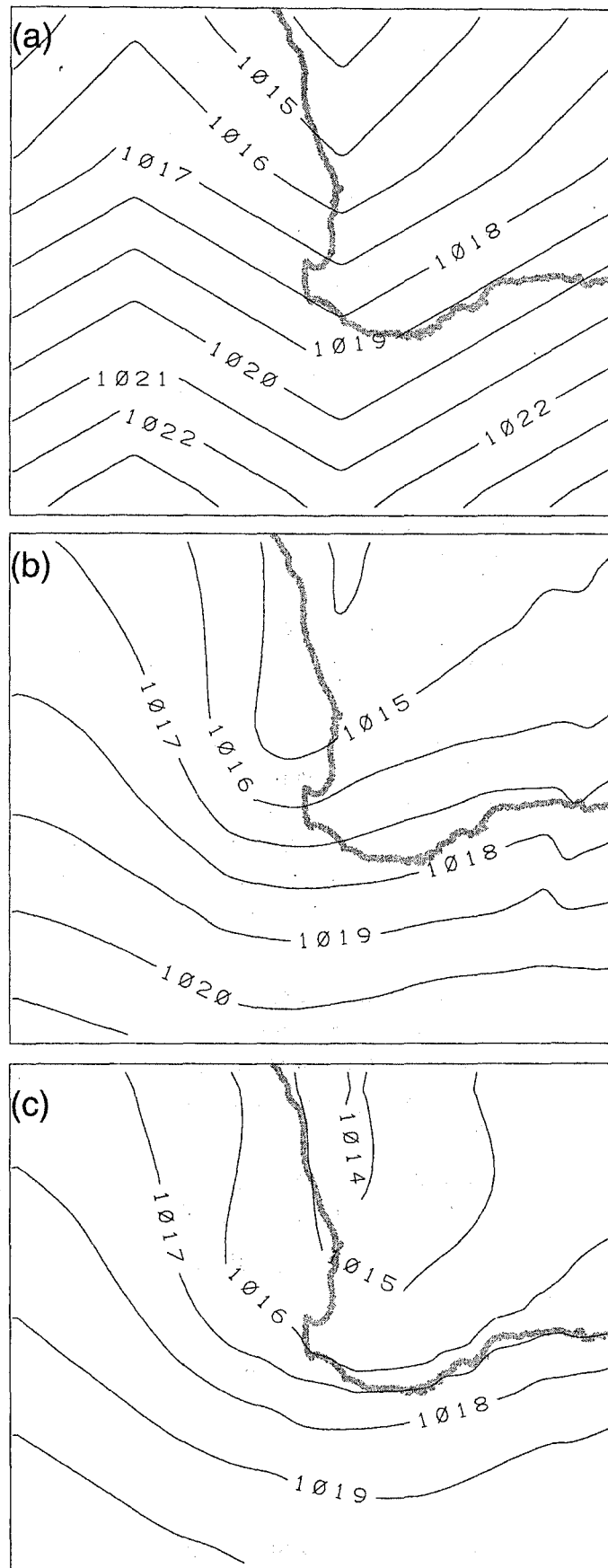


Figure 3. Surface pressures calculated by the model at (a) midnight, model initialisation time, (b) 6 a.m. on the following morning and (c) 6 p.m. the following evening.

The overall trough structure always formed spontaneously, and took on the same general form for a range of wind directions on both sides of the trough. Factors which were crucial in generation of an appropriate trough structure appeared to be

1. an initial temperature and wind profile for a morning when a trough axis was within about 100 km offshore. Without such a profile, the three-dimensional wind and stability structure generated by the model would not permit a trough to persist.
2. a significant turn of the gradient wind direction at the nominal trough axis (usually at least 60°). In the absence of such a change, a significant trough would often not stabilise at the coast.
3. a return to easterly or north easterly wind directions in the extreme western region of the grid. Cases where this feature was not included generated too strong a southerly to the west of the trough.

To produce the necessary motion inland of the trough at the required time, an additional forcing was usually required, in the form of an enhanced west-to-east pressure force. Typically, the surface gradient wind west of the trough was altered to a 10-15 m s⁻¹ southerly, over a period of 12 hours, with the value east of the trough reducing to an easterly of about 5 m s⁻¹.

When a satisfactory regional-scale representation had been generated, the model was rerun at higher resolution, using the earlier output to provide initial and lateral boundary conditions. The resolutions used have varied, typically being 3 km by 5 km or 6 km by 10 km.

4. Case Studies

The summer season of 1993-1994 was the period of most intensive monitoring during the Perth Photochemical Smog Study. Although the early part of the season produced less smog events than previously observed, a number occurred during February and March, and have proven worthwhile subjects for study.

Prior to March, extensive upper-level monitoring was possible, using radiosondes, a RASS radar system, two sodar units and aircraft surveys. These observations provided detailed meteorological data for use in model initialisation and validation.

However, at the start of March, the hired radiosonde equipment was returned, and the RASS system failed. This meant that the extent of available meteorological data was less. The sole vertical profile measurements were provided by twice- or three-times daily radiosonde measurements, made at Perth Airport, and the sodar wind measurements made at Cullacabardee.

The following case studies represent one day in the period when detailed data were available, and one during the March period when less measurements were made. Significantly, in both cases the extent of measurements was fully adequate to permit detailed investigation of model strengths and weaknesses.

4.1. 4 February 1994

The two weeks extending from late January were chosen as the period of most intensive work, with aircraft and vehicle-borne measurements, and expanded surface monitoring of smog precursors. The period did not include any days of high smog concentrations, but a close-to-normal meteorological pattern occurred on one day. The main shortcoming compared to the

norm was lower air temperatures, which led to lower than normal ozone concentrations. Peak values inland were in the range 50-65 ppb.

The low air temperatures also had significant effects within the model. In the southern region of the low-resolution grid, the combined effects of the measured temperatures at Perth and the normal southward decrease of air temperatures caused excessive atmospheric instability at the surface. The consequence was numerical instabilities, which prevented use of the normal low-resolution grid for the first stage of the simulation.

Attempts to simulate the effect of the trough by changing the pressure gradient to produce an onshore acceleration were also of arguable value. In figure 4, it can be seen that the onshore acceleration developed at all levels. Although the match between measured and modelled surface winds was improved, an invalid onshore acceleration also occurred at higher levels. This brought cooler air to the upper levels of the model, reducing stability and spuriously increasing mixing depths.

This effect is a direct consequence of the dynamics of all primitive equation models. Horizontal accelerations at all model levels reflect the effect of both the surface pressure gradient, and of the gradient of geopotential (derived from modelled temperatures). This means that applied surface pressure changes affect winds at all levels.

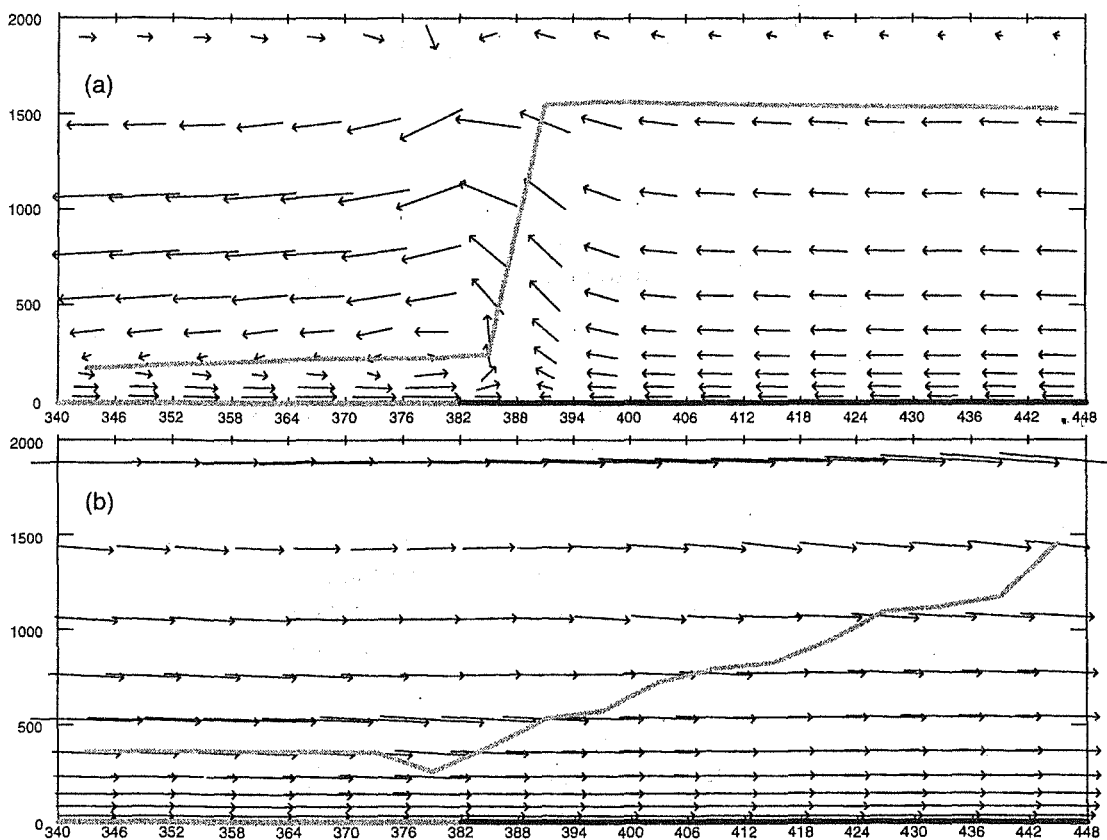


Figure 4. Effects of using surface pressure forcing, for the case study of 4 February 1994, at 1400 WST. The views correspond to west-east slices at AMG northing 6470 km. The transition from sea to land is indicated by a change from a broad shaded line to a broad black line, at the bottom of each figure. Mixing depth estimates are shown by the narrower shaded line. In (a), no forcing has been applied, and sea breeze arrival is delayed in comparison to measurement. In (b), some forcing has been used, but onshore winds have developed at all layers.

In principle, by combining a change of surface pressure with a compensating change of horizontal temperature gradient near the surface, the forcing of upper-level winds can be eliminated. However, while this feature has recently been implemented in the model, benefits are not yet clearly apparent.

Figure 4 illustrates the effects of pressure gradient forcing on model calculations for 4 February 1994. Figure 4(b) shows clearly the onshore turning of winds at all levels. Also shown in figure 4 are mixing depth estimates. Values inland, at the AMG easting of Caversham (403 km), are about 700 m. These are over 50% higher than those measured using radiosondes and the airborne sensors.

This difference appears to be due to two causes. One is the transport inland of cool air by the invalid upper-level inflow. Another is the generally warmer temperatures in the sea breeze inflow, compared to those which actually occurred as the coastal trough moved inland.

For the final model runs which were used to provide data for photochemical modelling, the effect of the cooler trough air was simulated by applying a uniform cooling of 6°C per day to the lower 6 model levels (extending to about 500 m). This arbitrary, but necessary, adjustment generated mixing depths in fair agreement with measurements.

4.2. 18 March 1994

The meteorology of this day proved relatively easy to model, with the slow advance inland of the front occurring without extra forcing. The first model run was performed at a grid resolution of 12 km by 40 km, using a grid of 120 cells west-east and 30 cells south-north. It was initialised with four regions of uniform gradient wind, separated by lines at AMG northing 6000 km (about 460 km south of Perth) and AMG easting 150 km (about 230 km offshore at Perth). Surface gradient wind speeds were all set at 15 kt, those in the north eastern quadrant from 40°, in the south eastern quadrant from 140°, in the south western quadrant from 320° and in the north western quadrant from 220°. The result was an initial offshore north-south trough, intersecting a west-east ridge south of the state.

The calculated fields showed a broad low pressure trough just over 100 km inland at midnight after 24 hours of model time, regressing to the coast and sharpening about sunrise (figure 5). This was close to the observed conditions for the day, so the midnight data set was used to initialise the high-resolution run, which used a 3 km by 5 km calculation grid.

A comparison of measured and calculated wind fields at 3pm for this run is shown in figure 6. The overall structure of the sea breeze, and the location of the sea breeze front, can be seen to be modelled well. Wind speeds and directions near the surface were also in close agreement with measurement (e.g., figure 7).

However, there was an apparently significant discrepancy of wind directions above 500 m height. The modelled directions at 1pm were between southerly and south easterly to about 1000 metres. Measurements showed directions close to north easterly.

This difference is consistent with differences between modelled and measured surface winds inland of the sea breeze front at 3pm (figure 6). These can be presumed to reflect the influence of winds between 500 and 1000 m, since mixing depth exceeded 1000 m inland of the sea breeze. Measured surface winds were from the north east, while modelled directions were from south of east.

The effects of this discrepancy were probably the source of differences between modelled mixing depths, and those based on Perth Airport measurements and the structure of the sodar

wind profile at Cullacabardee. Both sources of measurements suggested mixing depths in the 200 to 300 m range through most of the afternoon. Model calculations only reach this range at about 4pm, with earlier values reaching about 500 m over most of the region (figure 8).

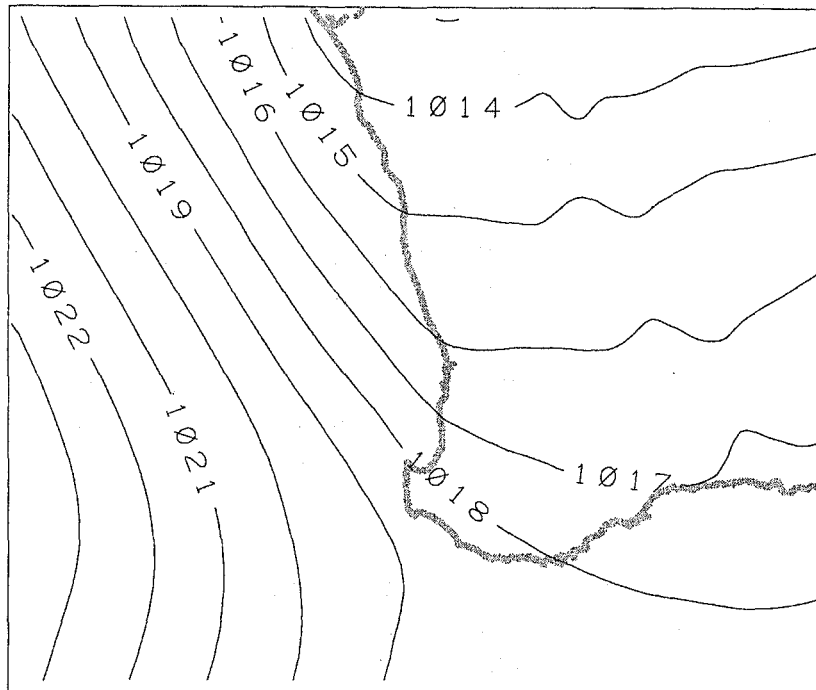


Figure 5. Surface pressure field at 8am on the second of modelled day of the low-resolution simulation for 18 March 1994.

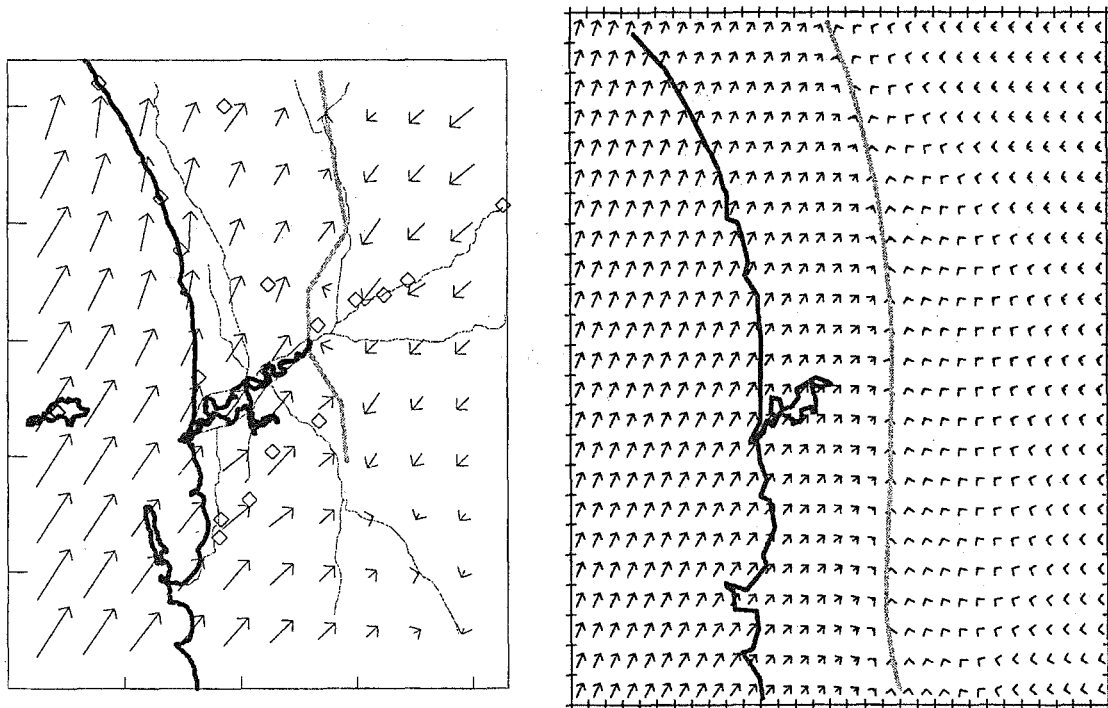


Figure 6. Comparison of windfields interpolated from measurements (left) and calculated by 3DSB (right), for 3pm on 18 March 1994. The maps are on the same scale, but wind vector length scales differ. The broad shaded line on each plot indicates the interpreted location of the sea breeze front.

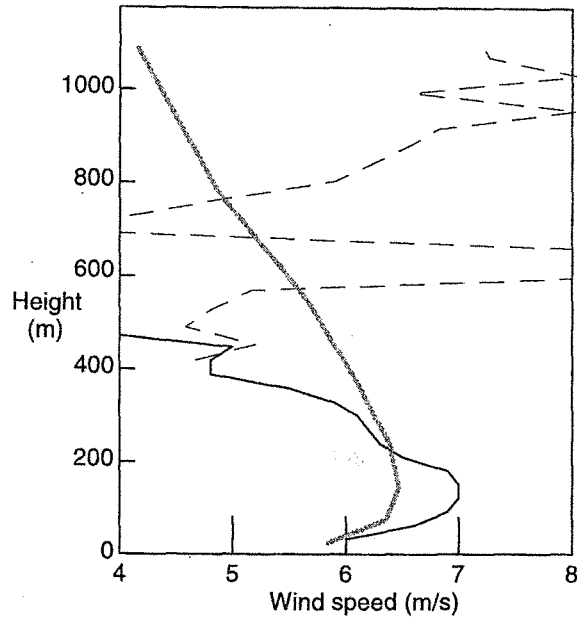


Figure 7. Wind speeds measured by the Cullacabardee sodar at 3 pm (solid line), Perth airport sonde at 1pm (dashed line) and modelled for the grid point nearest Cullacabardee (broad shaded line), on 18 March 1994. The sodar range limit is about 350-400 m, and measurements above this height range are suspect.

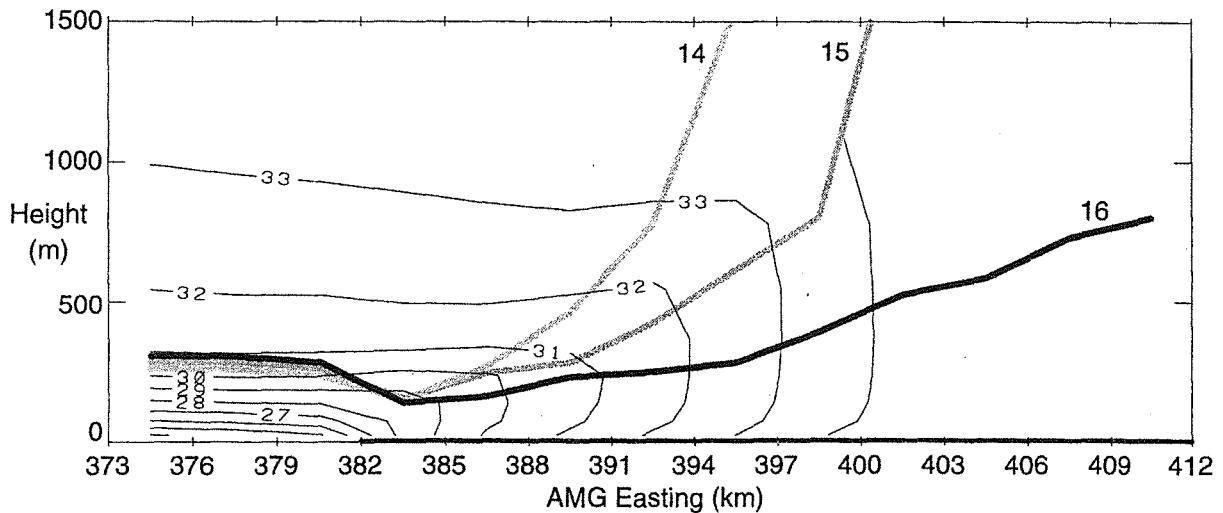


Figure 8. Mixing depth profiles at the latitude of Perth, calculated by 3DSB for hours 14, 15 and 16 WST on 18 March 1994. Contours of potential temperature at hour 15 WST are also shown.

5. Discussion

The primary area of concern in the application of the model to the Perth region was the effect of the pressure forcing, which was generally required to ensure the correct advance inland of the sea breeze front or coastal trough. Even when such forcing was not applied, in the case of 18 March 1994 (section 4.2), there were still apparent problems related to the accuracy of simulation of mixing depths.

Some work has subsequently been performed, in which the increased pressures offshore were compensated by a temperature decrease in the lowest 10 to 20% of the atmosphere. The result was zero acceleration above the cooled layer. Some test model runs have shown the expected increase of upper-level air temperatures, and decreases of inland mixing depths.

However, because of the shallower layer in which the pressure forcing has effect, a much stronger pressure change is required to generate the required onshore flow trend. Further study of the realism of these simulations is needed.

6. Conclusions

The numerical model described in this report has proven to have the capacity to represent the formation and inland movement of both sea breezes, and the coastal trough which forms near Perth during the summer season. However, to generate inland motion of the trough at the correct time, additional forcing in the form of an applied surface pressure gradient is generally required.

This forcing term also affects upper-level winds, and the consequent changes to upper-level air temperatures can reduce atmospheric stability, so altering mixing depth estimates inland. While it is possible to correct these trends within the model, it must be remembered that the end result is a physically-consistent reconstruction of the actual meteorological conditions, rather than an "à priori" simulation of a day's meteorology.

7. References

- Keppert, J.D. and R.K. Smith, 1972, "A simple model of the Australian West Coast Trough", *Monthly Weather Review*, **120**, 2042-2055.
- Pitts, R.O, and Lyons, T.J., 1988. "The Influence of Topography on Perth Radiosonde Observations", *Aust. Met. Mag.* **36**, 17-23.
- Rye, P.J., 1989, "Evaluation of a simple numerical model as a mesoscale weather forecasting tool", *J. Appl. Met.*, **28**, 1257-1270.
- Rye, P.J., 1996, "Modelling Perth photochemical smog events using the Urban Airshed Model", W.A. Department of Environmental Protection Technical Series 85.

APPENDIX

Detailed Description of the Model

The model was designed originally to provide a representation of the broader-scale processes within the sea breeze, so a simple, robust scheme was adopted. The hydrostatic scheme developed originally by Smagorinsky, Manabe and Holloway (1965) was used, in the form as modified by Kesel and described by Haltiner (1971). While the model has always possessed limitations, as a trade-off against computational performance, there have never been any limitations which could be traced to an inadequacy of this scheme.

On the other hand, its computational efficiency has allowed the model to be applied in circumstances where others were too slow for practical application. For example, in America's Cup forecasting applications, useful forecasts were obtained in 15 minutes on a MicroVAX II computer.

a. Finite Difference Scheme

The basic equations of motions were

$$\frac{dp_* u}{dt} = -p_* \frac{\partial F}{\partial x} - RT \frac{\partial p_*}{\partial x} + fp_* v + G_u + S_u + A_u + E_u \quad (\text{A1})$$

$$\frac{dp_* v}{dt} = -p_* \frac{\partial F}{\partial y} - RT \frac{\partial p_*}{\partial y} - fp_* u + G_v + S_v + A_v + E_v \quad (\text{A2})$$

$$\frac{\partial \Phi}{\partial \sigma} = -\frac{RT}{s} \quad (\text{A3})$$

$$\frac{\partial p_* T}{\partial t} = \left(\frac{2}{7}\right) T \left(\frac{w}{\sigma} + \frac{\partial p_*}{\partial t}\right) + G_T + S_T + A_T + E_T \quad (\text{A4})$$

$$w(\sigma_1) = -\frac{1}{p_*} \int_{\sigma_1}^{\sigma_2} \frac{dp_*}{dt} d\sigma \quad (\text{A5})$$

where u was eastward (x-component) velocity, v was northward (y-component) velocity, R was the gas constant ($287 \text{ J kg}^{-1} \text{ K}^{-1}$), Φ geopotential gz (for acceleration due to gravity g and height z), p_* surface pressure, f the Coriolis factor, σ was p/p_* for surface pressure p , T the temperature, w was $d\sigma/dt$, and G , S , A and E were contributions due to subgrid, surface and turbulent transfer, and turbulent entrainment, respectively.

Equations (A1) to (A5) were rendered into finite differences using a conservative flux formulation and leapfrog integration. For a detailed explanation of the numerical scheme, the reader is referred to Haltiner (1971). Values of all modeled variables were computed at grid centres.

While most three-dimensional models use equal grid sizes in both horizontal directions, experience showed this was not necessary for the current model. With a need for greater detail in the west-east (closely onshore) direction, the model resolution is normally higher in that direction. Typical grid element sizes were $3 \times 5 \text{ km}$ and $6 \times 10 \text{ km}$, but realistic large-scale trough simulations were generated using a $12 \times 80 \text{ km}$ grid. The horizontal extent of the model is arbitrary, but typical grid sizes were 120×30 and 60×40 points.

The model used 13 layers of thickness increasing with height, most rapidly above about 600 metres (the typical limit of sea breeze depth). The sigma profile used to define layers was

$$\sigma(k) = \exp(-0.005 k - 0.0002 k^3) \quad (\text{A6})$$

Model layers were centred approximately at 22, 72, 137, 228, 355, 530, 760, 1050, 1420, 1880, 2430, 3074 and 3820 metres.

b. Subgrid-scale Transfer

When symmetric differences are used to form gradient estimates, spurious short-wavelength features tend to form. These were filtered from the modelled fields by introduction of a diffusivity, giving a subgrid smoothing term of form

$$Gq = [DX_{i-1/2,k} (p_*q_{i-1,k} - p_*q_{i,k}) + D_{i+1/2,k} (p_*q_{i+1,k} - p_*q_{i,k})]/\Delta x^2 \\ [DY_{i,k-1/2} (p_*q_{i,k-1} - p_*q_{i,k}) + D_{i,k+1/2} (p_*q_{i,k+1} - p_*q_{i,k})]/\Delta y^2 \quad (\text{A7})$$

where q was any of u , v or T , each of the variables on the right was evaluated at $T-\Delta t$, for integration time step Δt , and

$$DX = 0.2|u/\Delta x| \quad (\text{A8})$$

$$DY = 0.2|v/\Delta y| \quad (\text{A9})$$

c. Boundary Conditions

The principal factor constraining the time step in hydrostatic models is the horizontal acoustic mode, in which horizontal divergence below a reflecting upper boundary excites oscillations obeying the linear sound propagation equations. This mode is usually filtered by constraining the horizontal divergence.

In the present case, a filter was chosen that would permit surface pressure changes, while still slowing the acoustic mode. The basis was the following modification of the tendency equation:

$$\frac{\partial p_*}{\partial t} = -\alpha \int_{\sigma_{\text{top}}}^1 \frac{\partial(p_*u)}{\partial x} d\sigma \quad (\text{A10})$$

where σ_{top} was the value of σ at the top of the highest model layer. Use of an α value of 1 corresponded to an unfiltered acoustic mode, and a value of zero to constant surface pressure. Experiment showed that choices for α in the range 0.05 to 0.10 did not affect surface pressure changes significantly, but allowed the computation time step to be increased by a factor of about four.

Conceptually, this boundary condition corresponded to a near-compensation of the integrated divergence within the model, by convergence in the layer above.

Changes in lateral boundaries were represented using an outward radiation condition, which gave for the time derivatives used in the integration step

$$\left. \frac{\partial q_b}{\partial t} \right|_t = C(p_*q_{i|_{t-\Delta t}} - p_*q_{b|_{t-\Delta t}}) / \Delta x \quad (\text{A11})$$

where q was u , v or T , C was the outwardly-directed wave velocity, and the subscripts b and i indicate the boundary and its adjacent interior points, respectively. Values of C up to 75 m s^{-1} resulted in a stable boundary, 40 m s^{-1} normally being used.

d. Surface Transfer

The flux of heat from the surface to the first model layer was derived from the surface-layer profiles laws of Garratt (1978) and Webb (1970). Changes to each variable were defined for layer 1 using

$$S_u = -p_* C_d U_1 u / \Delta z_1 \quad (\text{A12})$$

$$S_v = -p_* C_d U_1 v / \Delta z_1 \quad (\text{A13})$$

$$S_T = -p_* C_h U_1 \Delta \theta_0 / \Delta z_1 \quad (\text{A14})$$

where U_1 was wind speed and Δz_1 was the thickness of layer 1, and mean surface potential temperature excess $\Delta \theta_1$. Equations (A12) to (A14) required iterative solution of the following set of equations:

$$\text{friction velocity } U_* = C_d^{1/2} U_1 \quad (\text{A15})$$

$$\text{temperature flux } U_* \theta_* = C_h U_1 \Delta \theta_0 \quad (\text{A15})$$

Monin-Obukhov length

$$L = -\frac{U_*^3 \theta}{kg U_* \theta_*} \quad (\text{A16})$$

instability parameters

$$\Phi_m(z) = \begin{cases} 1 + 4.7z/L & L \geq z \\ 5.7 & 0 < L < z \\ (1 - 16z/L)^{-1/4} & L < 0 \end{cases} \quad (\text{A17})$$

$$\Phi_h(z) = \begin{cases} 1 + 4.7z/L & L \geq z \\ 5.7 & 0 < L < z \\ (1 - 16z/L)^{-1/2} & L < 0 \end{cases} \quad (\text{A18})$$

surface transfer coefficients from

$$\frac{k}{C_d} \bar{v}_z \begin{cases} \ln\left(\frac{z}{z_0}\right) + 4.7\left(\frac{z-z_0}{L}\right) & L \geq z \\ 4.7\left(1 - \frac{z_0}{L}\right) + 5.7 \ln\left(\frac{z_0}{L}\right) - \ln\left(\frac{z_0}{L}\right) & 0 < L < z \\ \ln\left(\frac{(1-\Phi_M)(1+\Phi_0)}{(1+\Phi_M)(1-\Phi_0)}\right) - 2 \tan^{-1}\left(\frac{\Phi_M - \Phi_0}{1 + \Phi_M \Phi_0}\right) & L < 0 \end{cases} \quad (\text{A19})$$

$$\frac{kC_d}{C_h}^{1/2} \begin{cases} \ln\left(\frac{z}{z_T}\right) + 4.7\left(\frac{z-z_T}{L}\right) & L \geq z \\ 4.7\left(1 - \frac{z_T}{L}\right) + 5.7 \ln\left(\frac{z_T}{L}\right) - \ln\left(\frac{z_T}{L}\right) & 0 < L < z \\ \ln\left(\frac{(1-\Phi_H)(1+\Phi_T)}{(1+\Phi_H)(1-\Phi_T)}\right) & L < 0 \end{cases} \quad (\text{A19})$$

where k was von Karman's constant, z_0 was surface roughness length and z_T was the roughness length for temperature exchange. Normally, the roughness length over land was taken to be 0.1 m, with changes by a factor two in either direction having no significant effect on the calculated winds and temperatures. Over water, Charnock's (1955) formulation was used, namely

$$z_0 = 0.014 u_*^2/g \quad (\text{A20})$$

Garratt's relation $z_T = z_0/7$ was used to define z_T .

Soil temperature changes were estimated using the force-restore method (e.g., Deardorff, 1978). The rate of change of surface temperature was given by

$$\frac{\partial T_0}{\partial t} = -(2\pi)^{1/2} H_A / (\rho_s C_s d_I) - 2\pi(T_0 - T_s) / \tau_1 \quad (\text{A21})$$

where the values of ρ_s , C_s and d_I were taken to be applicable to dry quartz sand (Deardorff, 1978, Table 2) and $\tau_1 = 86400$ s (1 day). The value of T_s used was obtained from climatic data (Bureau of Meteorology, 1966).

The effect of vegetation on the transfer of heat from the surface to the air was parameterised by an effective temperature excess, which was a fraction of the calculated soil surface temperature excess. Garratt's values for the Daly Waters region where his data were collected could be interpreted to give an estimate for this fraction of 0.36. Radiometric measurements conducted in midsummer, in the Kwinana region, near the coast south of Perth have shown a much larger fraction, of about 0.6. Since the events modelled are exclusively summer phenomena, the latter ratio has been used.

The term H_A was the net heat flux into the surface, given by the difference of net solar, long wave and terrestrial radiation and turbulent surface transfer terms.

Solar fluxes were based on the solar radiation model of Spencer (1972). The short-wavelength albedo estimates used Paltridge's (1971) solar-elevation dependent measurements. His data for normal sun incidence ranged from 0.14 to 0.23, with 0.2 being used in the model.

Long wave radiation was estimated using a clear-sky model, since weather conditions to which the model was applied were rarely cloudy. The model described by Washington and Williamson (1977, pages 152-160) was chosen, because of its ease of implementation. Due to the heavy computational demand of the model, and the slow change of radiation cooling rates, it was run once per hour of model time, with calculated rates used for the following hour.

While a more sophisticated approach could have been taken, the benefit of calculating long-wave radiation fluxes, over the basic alternative of imposing layer-average radiation cooling rates, proved small. Once the gross effect of long wave cooling had been included in the model, other factors such as advection dominated the heat budget.

Terrestrial radiation calculations used the Stefan-Boltzman law, presuming a surface emissivity of 0.9, an average of data presented by Weiss (1971).

The set of equations (A12) to (A21) may be solved iteratively at every timestep (e.g., Physick 1976). Since the resultant parameters approach equilibrium quickly and do not change greatly from one model timestep to the next, it was found that a single iteration per time step was sufficient.

e. Turbulent Transfer

Turbulent fluxes were derived from an eddy-diffusivity formulation, based on an extrapolation of surface layer expressions. The flux of each parameter was derived using an expression of form

$$A_q = \frac{\partial}{\partial z} \left(K_M \frac{\partial(p_* q)}{\partial z} \right) \quad (\text{A22})$$

where q was u or v ,

$$A_T = \frac{\partial}{\partial z} \left(K_T \frac{\partial(p_* \theta)}{\partial z} \right) \quad (\text{A23})$$

and

$$K_x = \frac{U_* l}{\Phi_x} \quad (\text{A24})$$

for dimensionless profile function Φ_x ("x" representing M or H, for momentum and heat, respectively) The mixing length, l , was expressed in the form

$$l = \begin{cases} kz(1 - z/h)^{3/2} & z < h \\ 0 & z \geq h \end{cases} \quad (\text{A25})$$

where h was mixing depth and the exponent $3/2$ was chosen to give acceptable agreement with measurements (e.g., Hanna 1978). Changes of the exponent used in (A25), within reasonable bounds, were found to have little effect on the development of the modeled sea breeze.

Likewise, the calculated winds showed little response to the form chosen to represent K_M and K , or to any presumed temperature gradient in the upper part of the convective layer. It was concluded that the sea breeze formed in response to the overall distribution of temperature in the atmospheric boundary layer, and the effects of any small differences in the vertical distribution of temperature inland were masked by the turbulent vertical mixing of momentum.

At levels above the mixed layer, turbulent transfer was generally zero. The sole exception resulted from the need to represent Kelvin-Helmholtz instability. This was presumed to develop when the Richardson number,

$$\text{Ri} = \frac{g}{\theta} \frac{\partial \theta}{\partial z} \left[\frac{\partial(u^2 + v^2)}{\partial z} \right]^{-2} \quad (\text{A26})$$

fell below 0.2 (Turner, 1973, pp. 94-107). In such cases, turbulent transfer between layers was computed using an eddy viscosity of

$$K_H = K_M = K_0 \frac{0.2 - \text{Ri}}{0.4 - \text{Ri}} \quad (\text{A27})$$

where $K_0 = 0.25 \Delta z^2 / \Delta t$, for model level separation Δz and time step Δt . This represented only a requirement of smooth development to a maximum value small enough to avoid computational instability.

For the accurate estimation of h inland in a sea breeze inflow, it was found that some representation of the effects of entrainment of cool air into rising plumes was needed. After Turner [1973, Eq. (6.1.3)], a $-5/3$ power law was used to express the decrease of plume temperature excess with height. The numerical expression of this process was based on an entrainment parameter, E , defined as

$$E = \frac{5}{3} \frac{z_{i,k} - z_{i,k-1}}{\frac{1}{2}(z_{i,k} + z_{i,k-1})} \quad (\text{A28})$$

from which the temperature of a rising plume was revised from layer to layer, in form

$$(\theta_p)_k = [(\theta_p)_{k-1} + E\theta_k](1+E)^{-1} \quad (\text{A29})$$

where θ_p was the temperature of the rising plume. The mixing depth was defined as the height at which θ_p fell below the potential temperature of the atmosphere, interpolated linearly between modelled values of θ .

The qualitative effect of the entrainment term in the mixing depth model was to permit the existence of stable stratification within the calculated inflow layer, inland, in approximate correspondence with observations. Turner's formulation was used because no equivalent based on field data for such conditions was available. There is some evidence supporting comparable initial behaviour of convective plumes in the laboratory and in the field (e.g., Young 1988).

Experiments showed that inclusion of θ_* in the estimation of θ_p had little effect on the computed mixing depth, so θ_p was initially set at the potential temperature of the first layer. Likewise, the cooling of plumes by entrainment by entrainment, (A29), had little effect on computed mixing depths except immediately inland from the coast.

Mixing depth in nonconvective conditions can be estimated using surface-layer scaling terms, based on the approach of Zilitinkevitch (1972), or on standard Ekman-layer principles. Using the modification of the coefficient for Zilitinkevitch's expression proposed by Brost and Wyngaard (1978), these may be expressed

$$h = 0.4 \left(\frac{u_* L}{|f|} \right)^{1/2}$$

$$h = \text{constant} \times \left(\frac{u_* L}{|f|} \right)$$

The value of "constant" in (A31) was determined from the equilibrium cross-isobar flow angle of the sea breeze to be 0.1. This value is less than found by other researchers, and it may be that some stability effects over water reduce the actual friction velocity below that estimated by the model.

f. Turbulent entrainment

Since the model was to be routinely applied in coastal air quality studies, an explicit representation of the contribution of turbulent entrainment to mixing depth was essential.

Heat flux through the inversion was parameterised in terms of surface heat flux. The ratio of entrainment flux to surface flux has been measured to be in the range 0.2 to 0.3 (e.g., Deardorff 1980), and a value of 0.25 was used.

In the model, the layer in which the modelled inversion was located was cooled at a rate equal to the above heat flux, divided by its depth. This layer, and layers below, were warmed at a rate equal to the entrained heat flux divided by the depth to its top.

Momentum entrainment was also represented, assuming that the implied exchange coefficients for momentum and for heat were the same. That for heat was based on the entrainment flux, divided by the difference in potential temperature between the layer containing the inversion, and the boundary layer minimum. The momentum flux was this ratio, multiplied by the difference in velocity between the layer containing the inversion, and the average of the layers below.

Tests of the significance of entrainment in prediction of offshore wind speeds indicated that the details of the parameterisation used were not critical. Typical speeds and directions were altered by less than 0.5 m s^{-1} and 5° when the entrainment coefficient was halved, and 1 m s^{-1} and 10° when the entrainment process was eliminated.

g. Initialisation

The model uses two sources of information for initialisation. A single vertical wind, temperature and humidity profile is required, and details of a surface gradient wind field, which may be nonuniform in time and space, may also be provided. If the latter is not provided, the model presumes the lowest layer of the wind profile corresponds to the surface gradient wind.

To ensure a close balance of the initial wind and temperature field, so the model can be run stably over a period of several days, horizontal temperature gradients are calculated using the thermal wind equation. The formulation used, in the model's sigma coordinate system, is as follows:

$$\frac{\partial \Phi}{\partial x} = f \left(v - \frac{T v_{\text{surface}}}{T_{\text{surface}}} \right) \quad (\text{A32})$$

$$\frac{\partial \Phi}{\partial y} = -f \left(u - \frac{T u_{\text{surface}}}{T_{\text{surface}}} \right) \quad (\text{A33})$$

$$\frac{\partial T}{\partial x} = -\frac{\sigma}{R} \frac{\partial}{\partial \sigma} \left(\frac{\partial \Phi}{\partial x} \right) \quad (\text{A34})$$

$$\frac{\partial T}{\partial y} = -\frac{\sigma}{R} \frac{\partial}{\partial \sigma} \left(\frac{\partial \Phi}{\partial y} \right) \quad (\text{A35})$$

where the subscript "surface" indicates values for model level 1. The above relationship was applied at model levels for which σ was less than 0.95, constant gradients of zero eastward and $0.3 \text{ K}/100 \text{ km}$ northward being assumed near the surface.

References

- Brost, R.A. and J.C. Wyngaard 1978, "A model study of the stably stratified planetary boundary layer", *J. Atmos. Sci.* **35**, 1427-1440.
- Bureau of Meteorology, 1966, "Climatic Survey, Region 15 - Metropolitan Western Australia", Aust. Bur. Meteor., Melbourne.

- Charnock, H., 1957, "Wind stress on the water surface", *Quart. J. Roy. Meteor. Soc.*, **81**, 639-640.
- Deardorff, J.W., 1978, "Efficient prediction of ground surface temperature and moisture, with inclusion of a layer of vegetation", *J. Geophys. Res.*, **73**, 2549-2557.
- Deardorff, J.W., 1980. "Laboratory study of entrainment rate in a convectively mixed layer", Third Conference on Ocean-Atmosphere Interaction, Jan 30 - Feb. 1, Los Angeles, Calif.
- Haltiner, G.J., 1971, *Numerical Weather Prediction*, John Wiley and sons, 238-247.
- Hanna, S.R., 1978, "A review of the influence of new boundary layer results on diffusion prediction techniques", W.M.O. Symposium on the Application of New Boundary Layer Techniques to Air Pollution Modelling, W.M.O., Norrkoping, 119-126.
- Garratt, J.R., 1978. "Transfer characteristics for a heterogenous surface of large aerodynamic roughness", *Quart. J. Roy. Meteor. Soc.*, **104**, 491-502.
- Haltiner, G.J., 1971, *Numerical Weather Prediction*, John Wiley and Sons, 238-247.
- Paltridge, G.W., 1971. "Solar and thermal radiation flux measurements over the east coast of Australia", *J. Geophys. Res.*, **76**, 2857-2865
- Physick, W.L., 1976, "A numerical model of the sea breeze phenomenon over a lake or gulf", *J. Atmos. Sci.*, **33**, 2107-2135.
- Rye, P.J., 1989, "Evaluation of a simple numerical model as a mesoscale weather forecasting tool", *J. Appl. Met.*, **28**, 1257-1270.
- Smagorinsky, J., S. Manabe and J.L. Holloway, 1965, "Numerical results from a nine-level general circulation model of the atmosphere", *Mon. Wea. Rev.* **93**, 727-768.
- Spencer, J.W., 1972. "Computer estimation of direct solar radiation on clear days", *Solar Energy*, **13**, 437-438.
- Turner, J.S., 1973, "Buoyancy Effects in Fluids", Cambridge University Press.
- Washington, W.M. and D.L. Williamson, 1977. "A description of the NCAR global circulation models", *Methods in Computational Physics* **17**, 111-172.
- Weiss, M., 1971. "Airborne measurements of earth surface temperature ocean and land in the 10-12... and 8-14 μ regions", *Appl. Opt.*, **10**, 1280-1287.
- Webb, E.K., 1970. "Profile relationships: the log-linear range, and extension to strong stability", *Quart. J. Roy. Meteor. Soc.*, **96**, 67-90.
- Young, G.S., 1988, "Turbulence structure of the convective boundary layer. part i: variability of normalized turbulence statistics", *J. Atmos. Sci.* **33**, 719-726.
- Zilintinkevitch, S.S., 1972. "On the determination of the height of the Ekman boundary layer", *Bound. Layer Met.* **3**, 141-145.